Advanced Optical Materials

ADVANCED OPTICAL MATERIALS
www.advopticalmat.de

RESEARCH ARTICLE OPEN ACCESS

WS_2 Micro-Dome Single Photon Source in a Tunable Open Cavity

Jens-Christian Drawer[1] | Salvatore Cianci[2] | Vita Solovyeva[1] | Alexander Steinhoff[1] | Christopher Gies[1] | Falk Eilenberger[3,7] | Kenji Watanabe[4] | Takashi Taniguchi[5] | Ivan Solovev[1] | Giorgio Pettinari[6] | Federico Tuzi[2] | Elena Blundo[2] | Marco Felici[2] | Antonio Polimeni[2] | Martin Esmann[1] | Christian Schneider[1]

[1]Institut für Physik, Fakultät V, Carl von Ossietzky Universität Oldenburg, Oldenburg, Germany | [2]Physics Department, Sapienza University of Rome, Rome, Italy | [3]Institute of Applied Physics, Abbe Center of Photonics, Friedrich Schiller University Jena, Jena, Germany | [4]Research Center for Electronic and Optical Materials, National Institute for Materials Science, Tsukuba, Japan | [5]Research Center for Materials Nanoarchitectonics, National Institute for Materials Science, Tsukuba, Japan | [6]Institute for Photonics and Nanotechnologies, National Research Council, Rome, Italy | [7]Fraunhofer-Institute for Applied Optics and Precision Engineering IOF, Jena, Germany

Correspondence: Christian Schneider (christian.schneider@uni-oldenburg.de)

Received: 6 November 2025 | **Revised:** 14 July 2026 | **Accepted:** 7 August 2026

Keywords: H-ion irradiation | open microcavities | quantum dots | single-photon sources | two-dimensional materials

ABSTRACT

Versatile, tunable, and potentially scalable single-photon sources are a key asset in emergent photonic quantum technologies. In this work, a single-photon source based on WS_2 micro-domes, created via hydrogen ion irradiation, is realized and integrated into an open, tunable optical microcavity. Single-photon emission from the coupled emitter–cavity system is verified via the second-order correlation measurement, revealing a $g^{(2)}(\tau = 0)$ value of 0.3. A detailed analysis of the spectrally selective, cavity enhanced emission features shows the impact of a pronounced acoustic phonon emission sideband, which contributes specifically to the non-resonant emitter–cavity coupling in this system. The achieved level of cavity–emitter control highlights the potential of open-cavity systems to tailor the emission properties of atomically thin quantum emitters, advancing their suitability for real-world quantum technology applications.

1 | Introduction

Compact and efficient sources of quantum light are of critical importance in establishing quantum communication networks and are advancing as building blocks in on-chip quantum information processing. In recent years, a large palette of solid-state single-photon emitters has emerged, featuring different degrees of flexibility and versatility. While InAs-based quantum dots still perform best in terms of single-photon emission brightness and purity, atomically thin semiconductors are promising candidates as a versatile, scalable, and low-cost alternative. Thus far, single-photon emission was demonstrated from localized exciton emitters in strained transition-metal dichalcogenide (TMDC) mono- and bilayers [1–4], He^+ ion beam–irradiated MoS_2 monolayers [5, 6], as well as moiré-trapped excitons in van der Waals heterostructures [7]. In a recent work, the feasibility of creating micro-domes via hydrogen ion beam irradiation of thin TMDC thin flakes was demonstrated, which represents a novel degree of freedom in engineering both the global and the local strain in van der Waals heterostructures [8, 9]. It was furthermore demonstrated that such micro-domes can host single-photon emitters, rendering them

[Correction added on September 4, 2026, after first online publication: Affiliation 7 was incorrectly included for the author Christian Schneider and has instead been added for the author Falk Eilenberger.]

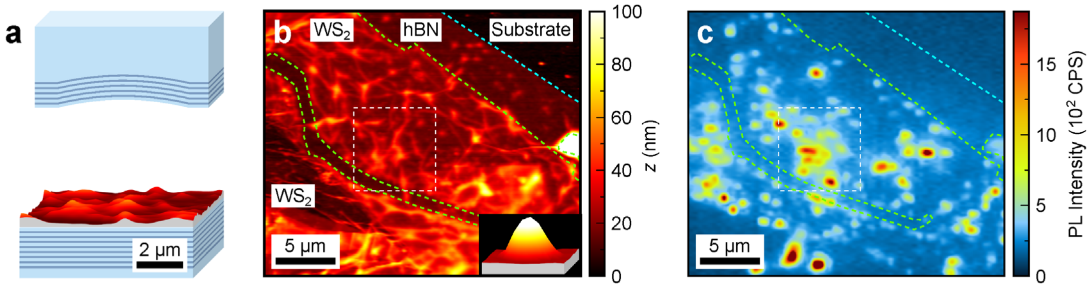

FIGURE 1 | (a) To-scale schematic of the ~5 µm long open cavity containing the hydrogenated and hBN-capped WS_2 layer. The topography of the active layer is scaled by a factor of 10 in the z direction. (b) AFM measurement of the hBN-capped, hydrogenated WS_2 layer. The edges of the WS_2 layer are indicated by a dashed green line, one of the edges of the hBN layer on top of it is shown by the dashed blue line, and the part shown in (a) is indicated by a dashed white square. An inset at the bottom right shows a dome before it was capped with hBN. It is scaled by a factor of 1.5 compared to (a). (c) PL map matching the region shown in (b), displaying the spectrally integrated intensity in the 622–650 nm range under 532 nm continuous wave laser excitation.

a unique approach toward deterministic sources of quantum light [10, 11].

In this work, we realize a cavity-tunable single-photon source based on a WS_2 micro-dome realized via hydrogen ion irradiation. We demonstrate quantum light emission from the deterministically coupled emitter–cavity system, and, via combining spectrally selective emitter–cavity coupling with an adapted model accounting for phonon degrees of freedom, we explore the effects of strong phonon sidebands of the 2D material coupled to the optical resonator mode [12, 13]. The main novelty of our work consists of two points: We combine a passively stabilized open cavity platform in a closed cycle cryostat with WS_2 micro-dome emitters, which has large implications for up-scaling TMD-based single photon sources. Our study furthermore captures the fingerprints of pronounced phonon sideband effects in the cavity–emitter coupling, thereby revealing the strong quenching of the cavity emission when brought in resonance with the emitter zero phonon line, which has previously only been reported in III-V materials.

2 | Methods and Results

The device consists of a hydrogenated WS_2 flake, which is integrated into a spectrally tunable, open Fabry–Pérot cavity (see Figure 1a). The lower mirror is a distributed Bragg reflector (DBR) made of 10.5 pairs of TiO_2/SiO_2, terminated with a SiO_2 layer, with optical layer thicknesses chosen as $\lambda/4$, such that the optical stop band is centered at 620 nm. A nominally 5 nm thick flake of WS_2, exfoliated from the bulk crystal by the Scotch-tape method, is transferred to the mirror using the dry-gel stamping technique. The low-index termination of the DBR places the WS_2 layer at a cavity-field antinode, hence no additional spacer layer is needed. This step is followed by the low-energy hydrogen beam irradiation procedure described in Reference [8, 14], which results in the formation of one-atomic-monolayer-thick domes that evolve at the surface of the flake. The deterministic placement of individual WS_2 domes by selective hydrogenation is possible [11] but was not performed here in favor of maximizing the number of emitters by globally covering the sample with micro-domes and relying on the flexible open microcavity as a complementary approach for emitter selection. Finally, the sample is capped with an approximately 8 nm thick layer of hexagonal boron nitride (hBN), making the domes mechanically stable even at cryogenic temperatures [11].

The top mirror consists of 5.5 layers of TiO_2/SiO_2, and lateral optical mode confinement is provided by a spherical-cap-shaped indentation (diameter of 6 µm, depth of 330 nm). More details can be found in Section S1.

First, we characterized the properties of the active hydrogenated WS_2 before mounting the cavity top mirror. Atomic force microscopy (AFM) measurements of the hBN-capped, hydrogenated WS_2 layer are shown in Figure 1b and the inset of Figure 1b displays a dome before hBN capping. While the uncapped dome features a highly symmetric shape, the topography on the hBN surface is strongly modified by formation of wrinkles in the capping layer. Figure 1c displays a spatially resolved micro-photoluminescence (PL) map of the studied flake, recorded at a sample temperature of 3.9 K using a confocal microscopy configuration without the top mirror. The sample flake is excited non-resonantly via an expanded 532 nm continuous wave diode laser. The spectrally integrated intensity in the emission window 622–650 nm is displayed, where we expect the luminescence from localized emitters in WS_2 domes [11]. We find that the PL emitted from the sample is highly anisotropic and localized; spot-like emission arises at positions that we assign to the occurrence of micro-domes.

Cavity coupling of single emission centers is accomplished by mounting the top distributed Bragg reflector in our open cavity framework. Since we can laterally align the two mirrors with nanometer-scale precision, it is possible to deterministically place a pre-selected emitter underneath the center of the spherical-cap-shaped indentation in the top DBR. Figure 2a displays a map of PL spectra for 532 nm continuous wave laser excitation that were recorded as the vertical distance between top and bottom DBRs was continuously tuned in a range between 4.98 µm and 5.44 µm. The primary, narrow-band emission signal of the localized emitter remains spectrally stable at an energy of 1.962 eV (labeled as X in Figure 2a). For negative cavity–emitter detunings (i.e., $E_c - E_x < 0$, where E_c is the energy of the cavity resonance, and E_x is the energy of the localized exciton), non-resonant emitter–cavity coupling [15] gives rise to a weaker, but distinct, luminescence

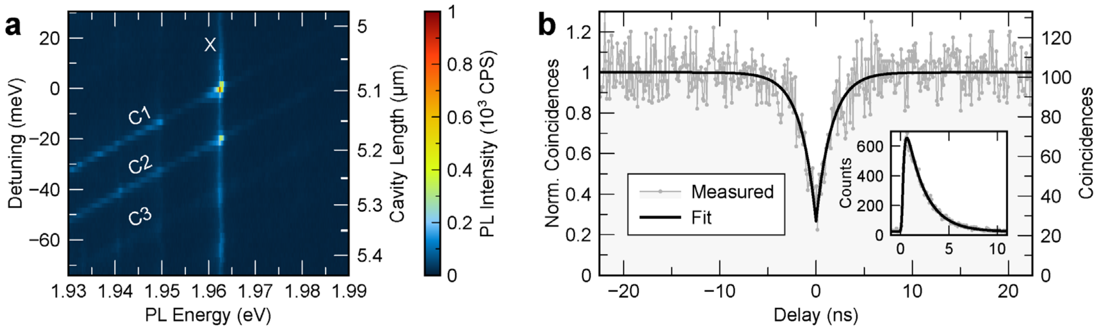

FIGURE 2 | (a) PL spectra for various detunings between cavity resonance energy and emitter energy, denoted as X, at approximately 1.962 eV. The diagonal features correspond to the spectrally tunable cavity modes, labeled C1–C3. On resonance (zero detuning), the intensity is enhanced by approximately a factor of 17. (b) Second-order correlation measurement at zero detuning, yielding $g^{(2)}(0) = 0.27 \pm 0.08$. The inset shows a lifetime measurement of the coupled system.

signal of the optical resonances of our cavity, with a linewidth of ~2.3 meV (labeled as C1 in Figure 2a). As we change the cavity length, the resonant mode can be fully tuned through the discrete, localized emission line, yielding a significant enhancement of the detected PL signal, up to a factor of approximately 17. We also detect higher-order cavity modes with energies 20 meV and 42 meV above the ground mode (labeled as C2 and C3 in Figure 2a, respectively), corresponding to higher-order Laguerre-Gaussian modes trapped in the plano-concave micro-cavity [16, 17]. The higher-order modes display less pronounced coupling behavior, since C2 features a field node in the lateral center of the photonic trap, and both C2 and C3 exhibit increased scattering losses compared to C1 due to their larger mode diameters. It is worth pointing out that, for positive detunings ($E_c - E_x > 0$), the emission from the cavity mode is strongly reduced as a result of a strong spectral asymmetry in the acoustic phonon sideband [18], which we investigate more closely later in this paper.

Single-photon emission from the resonantly coupled emitter–cavity system (zero detuning conditions) is verified by measuring the second-order correlation in a Hanbury–Brown and Twiss (HBT) setup under continuous wave and non-resonant excitation. We use a coarse spectral bandpass to filter the 600–650 nm window containing the primary emission feature, and couple the signal into a single mode fiber via a zoom collimator to allow optimal mode matched coupling. For the HBT measurement, a 50:50 fiber beam splitter is used with each output connected to an avalanche photodiode, both of which are connected to a time correlation device. The resulting correlation histogram, shown in Figure 2b, clearly displays a pronounced dip at zero time delay, which is the hallmark of non-classical light emission. The fit of the model $g^{(2)}(\tau) = 1 - p \cdot e^{-|\tau|/\tau_1}$, convoluted with the system response function, yields $g^{(2)}(0) = 0.27 \pm 0.08$, verifying the single-photon nature of the emission from our device. This value of the second-order autocorrelation is on par with the current state of the art in WS_2-based single-photon emitters [11, 19, 20]. We furthermore stress that we measured the $g^{(2)}$ with extremely coarse spectral filtering, only rejecting the excitation laser with a 50 nm wide band pass (600–650 nm) and the emitter near the center of the pass band at 632 nm. We thus expect further improvement of the $g^{(2)}$ by narrower spectral filtering, but this was not necessary here due to the excellent spectral isolation of the observed emitters.

The inset of Figure 2b shows a lifetime measurement of the emitter for pulsed 532 nm excitation when the emitter is in resonance with the cavity (8 µW focused intensity, ~5 ps pulse duration). Due to the required long integration times, the investigated emitters tended not to withstand a full, systematic investigation of lifetimes vs. detuning. Hence, we do not provide off-resonant lifetime measurements here. When emitters bleached, this happened abruptly. Likely origins are therefore not exclusively electronic in character. Instead, the mechanical instability of some domes should be deemed as the main cause of the emitter vanishing when the domes are exposed to high power densities in pulsed excitation studies. We model the setup response with a skewed Gaussian function and deconvolute the data by fitting the ideal model convoluted by the setup response function, yielding a characteristic decay time of $\tau_1 = 1.954 \pm 0.024$ ns (see Section S2C for details).

The highly tunable nature of our open cavity system allows us to gain further insight into the intricate interplay between the resonant coupling between cavity, quantum emitter, and phonon modes. To this end, we selected another emitter from a different dome, featuring a pronounced coupling with the lattice vibrations. In Figure 3a, we display high-resolution emission spectra of a selected emitter for strong (top panel) and modest (middle panel) negative detunings, as well as slightly positive detuning (bottom panel). The emission feature of this selected emitter is split into a doublet of discrete emission lines (zero-phonon lines, ZPLs), resulting from the inherent fine-structure of the apparent charge-neutral, localized exciton. As mentioned, the emitter has a pronounced acoustic phonon sideband (PSB) that emerges from phonon emission events at energies below the ZPL. As in the discussion of Figure 2a, we notice that the emission of the cavity mode is clearly visible for modest negative detuning, while it carries a substantially lower intensity at positive detuning, since phonon absorption events are strongly reduced at the chosen sample temperature of 4 K. Also, we found the doublet emission feature to be common and investigated its PL with respect to polarization. Figure S3 shows a representative measurement, revealing a high degree of linear polarization for each line and predominantly cross-polarization between the two lines.

In order to carry out a quantitative analysis, we have extended the model that was introduced in Reference [21] to describe the two

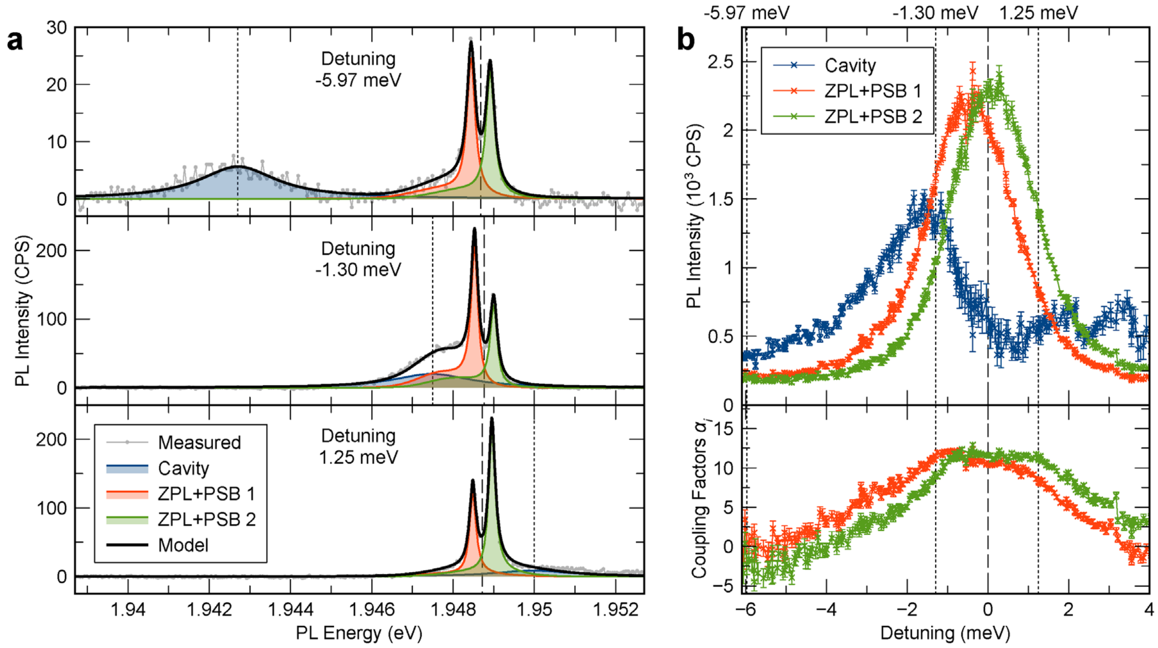

FIGURE 3 | (a) Measured PL spectra for three cavity emitter detunings with the fitted model, as well as its individual constituents, namely, the cavity and the lower (higher) energy emission feature "ZPL+PSB 1" ("ZPL+PSB 2"). (b) Integrated intensities attributed to the three modeled components (top) and the cavity emitter coupling factors (bottom) as a function of the cavity emitter detuning. The vertical thin dashed lines correspond to the three spectra shown in (a).

individual ZPL-PSB constituents of the spectra by the influence of the cavity as detailed in Reference [18]. In this approach, the spectral shapes of the ZPL $I_{\mathrm{ZPL}}(E)$ and of the cavity mode $I_{\mathrm{c}}(E)$ are described by Lorentzians, and the acoustic-phonon sideband (PSB) contribution is given by [21]

$$I_{\mathrm{PSB}}(E) = a \exp\left[-\left(\frac{E - E_{\mathrm{x}}}{\gamma_{\mathrm{ph}}}\right)^2\right] \times \left(\Theta(E_{\mathrm{x}} - E) + \frac{1}{\exp\left(\frac{|E-E_{\mathrm{x}}|}{k_{\mathrm{B}}T}\right) - 1}\right)|E - E_{\mathrm{x}}|, \quad (1)$$

where the temperature is $T = 4\,\mathrm{K}$.

For spectra with a significantly red-detuned cavity, any interaction beyond a simple additive superposition of the constituents is neglected, and a fit of type

$$I(E) = \sum_{i=1,2} \left(I_{\mathrm{ZPL},i}(E) + I_{\mathrm{PSB},i}(E)\right) + I_{\mathrm{c}}(E) + c \quad (2)$$

can be performed for each individual spectrum to extract the intensities, energies, and linewidth of the cavity mode, as well as the quantum emitter features. The index $i = 1$ ($i = 2$) corresponds to the lower (higher) energy emission feature of ZPL and PSB. Finally, the entire set of spectra for different cavity detunings is described with an individually fitted set of the remaining parameters, that is, the width of the ZPL Lorentzians $I_{\mathrm{ZPL},i}$, their average center energy $\frac{E_{\mathrm{x},1}+E_{\mathrm{x},2}}{2}$, and the amplitude of the cavity feature I_{c}. To this end, the adapted model

$$I(E) = \sum_{i=1,2} \left(I_{\mathrm{ZPL},i}(E) + I_{\mathrm{PSB},i}(E)\right) \cdot [1 + \alpha_i I'_{\mathrm{c}}(E)] + I_{\mathrm{c}}(E) + c \quad (3)$$

is employed, where I'_{c} is the normalized cavity mode intensity $I'_{\mathrm{c}} \equiv \frac{I_{\mathrm{c}}}{I_{\mathrm{c}}(E=E_{\mathrm{c}})}$. The expression given by Equation 3 accounts for the leaky emission of the two lines for far detuned cavity energies and describes how the cavity preferentially enhances the emission of the line that lies closer to its resonance. In contrast to Reference [18], two additional coupling factors α_i are introduced as fit parameters, which are shown in Figure 3b (bottom). They capture the deviation from the cavity acting as a purely multiplicative filter on the emission lines, allowing for better reproduction of the complete cavity length scan and improving the extraction accuracy of the individual components, whose integrated intensities are then given by

$$I_{\mathrm{c,Int}} = \int_{-\infty}^{\infty} I_{\mathrm{c}}(E)\mathrm{d}E, \quad (4)$$

$$I_{\mathrm{ZPL+PSB},i,\mathrm{Int}} = \int_{-\infty}^{\infty} \left(I_{\mathrm{ZPL},i}(E) + I_{\mathrm{PSB},i}(E)\right) \cdot \left[1 + \alpha_i I'_{\mathrm{c}}(E)\right]\mathrm{d}E, \quad i = 1, 2, \quad (5)$$

and which are shown in Figure 3b (top). From matching the measured spectra to our model, we obtain an average linewidth for the ZPL Lorentzians of $\mathrm{FWHM}_{\mathrm{ZPL},i} = 0.2054 \pm 0.0004\,\mathrm{meV}$. For an extensive step-by-step description of the fitting procedure, refer to Section S3.

The emitter in Figure 2 has a simple line structure that is easy to understand. It exhibits PL enhancement when brought into resonance with the multiple transversal modes of the open cavity. In contrast, the emitter in Figure 3 has a richer spectrum. Nevertheless, our quantitative model in Equation 3 is able to capture it in great detail. For completeness, we performed a second order autocorrelation of the emitter in Figure 3 (see Figure S4) and show the cavity tuning series for the emitter in Figure 3 (see Figure S5), i.e., the dataset analogous to the tuning in Figure 2a.

The central result of our data analysis reveals that the phonon-sideband emission funnels into the optical cavity mode, yielding the peculiar, strongly asymmetric intensity distribution of the cavity that peaks at slightly negative detunings. Interestingly, while the intensity of the ZPL reaches its maximum at zero-detuning, effectively, the intensity of the cavity mode undergoes a minimum, which is analogous to findings for single InAs quantum dots coupled to micropillar cavities [22] but which has not yet been observed for van der Waals quantum emitters.

3 | Conclusion

Our work demonstrates a micro-dome single-photon source in a tunable, open optical cavity. We explore the main spectral fingerprints of the micro-dome quantum emitters and their coupling behavior to the resonator. In particular, we find pronounced phonon-sideband emission, which yields significant non-resonant emitter–cavity coupling under negative detuning conditions, similar to observations in WSe_2 emitters in wrinkles [18]. Furthermore, we observe a strong quenching of the cavity mode intensity when the system is on resonance. Since micro-dome quantum emitters can be generated deterministically in TMDC flakes, our work outlines the possibility for a scalable implementation of spatially and spectrally deterministic TMDC-based single-photon sources. The pronounced exciton–phonon coupling also makes micro-dome single-photon sources interesting candidates for applications in quantum-optomechanics [23, 24].

Acknowledgements

This project was funded by the Deutsche Forschungsgemeinschaft (DFG, German Research Foundation), grant numbers INST 184/222-1 FUGG, INST 184/234-1 FUGG, INST 184/235-1 FUGG, and Gi1121/4-2. This project was funded within the QuantERA II programme that has received funding from the European Union's Horizon 2020 research and innovation programme under Grant Agreement No. 101017733, and with funding organization the Germany Federal ministry of research, technology and aeronautics, the Italian Ministry of University and Research, and the National Research Council of Italy within the project EQUAISE. The Niedersächsisches Ministerium für Wissenschaft und Kultur within the collaborative project DyNano is acknowledged. We gratefully acknowledge funding by the BMFTR within the project Tublan (FKZ 16KISQ089 and FKZ 16KISQ088). AP and MF acknowledge funding from the PNRR MUR project PE0000023-NQSTI (the National Quantum Science and Technology Institute). KW and TT acknowledge support from the JSPS KAKENHI (Grant Numbers 21H05233 and 23H02052), the CREST (JPMJCR24A5), JST and World Premier International Research Center Initiative (WPI), MEXT, Japan. The authors thank Heiko Knopf for his assistance with sample fabrication. The authors thank Ilaria Rago and Francesco Pandolfi for support with the AFM measurements.

Open access funding enabled and organized by Projekt DEAL.

Conflicts of Interest

The authors declare no conflicts of interest.

Data Availability Statement

The data that support the findings of this study are available from the corresponding author upon reasonable request.

References

1. A. Srivastava, M. Sidler, A. V. Allain, D. S. Lembke, A. Kis, and A. Imamoğlu, "Optically Active Quantum Dots in Monolayer WSe_2," *Nature Nanotechnology* 10, no. 6 (2015): 491.

2. M. Koperski, K. Nogajewski, A. Arora, et al., "Single Photon Emitters in Exfoliated WSe_2 Structures," *Nature Nanotechnology* 10, no. 6 (2015): 503.

3. Y.-M. He, G. Clark, J. R. Schaibley, et al., "Single Quantum Emitters in Monolayer Semiconductors," *Nature Nanotechnology* 10, no. 6 (2015): 497.

4. C. Chakraborty, L. Kinnischtzke, K. M. Goodfellow, R. Beams, and A. N. Vamivakas, "Voltage-Controlled Quantum Light from an Atomically Thin Semiconductor," *Nature Nanotechnology* 10, no. 6 (2015): 507.

5. J. Klein, L. Sigl, S. Gyger, et al., "Engineering the Luminescence and Generation of Individual Defect Emitters in Atomically Thin $MoSe_2$," *ACS Photonics* 8, no. 2 (2021): 669.

6. K. Barthelmi, J. Klein, A. Hötger, et al., "Atomistic Defects as Single-Photon Emitters in Atomically Thin $MoSe_2$," *Applied Physics Letters* 117, no. 7 (2020): 070501.

7. H. Baek, M. Brotons-Gisbert, Z. X. Koong, et al., "Highly Energy-Tunable Quantum Light from Moir'e-Trapped Excitons," *Science Advances* 6, no. 37 (2020): eaba8526.

8. D. Tedeschi, E. Blundo, M. Felici, et al., "Controlled Micro/Nanodome Formation in Proton-Irradiated Bulk Transition-Metal Dichalcogenides," *Advanced Materials* 31, no. 44 (2019): 1903795.

9. E. Blundo, F. Tuzi, M. Cuccu, et al., "Giant Light Emission Enhancement in Strain-Engineered InSe/MS_2 (M = Mo or W) van der Waals Heterostructures," *Nano Letters* 25, no. 9 (2025): 3375.

10. S. Cianci, E. Blundo, M. Felici, A. Polimeni, and G. Pettinari, "Tailoring the Optical Properties of 2D Transition Metal Dichalcogenides by Strain," *Optical Materials* 125 (2022): 112087.

11. S. Cianci, E. Blundo, F. Tuzi, et al., "Spatially Controlled Single Photon Emitters in hBN-Capped WS_2 Domes," *Advanced Optical Materials* 11, no. 12 (2023): 2202953.

12. A. Steinhoff, S. Wilksen, I. Solovev, C. Schneider, and C. Gies, "Impact of Phonon Lifetimes on the Single-Photon Indistinguishability in Quantum Emitters Based on Two-Dimensional Materials," *Physical Review B* 111, no. 19 (2025): 195431.

13. L. Vannucci, J. F. Neto, C. Piccinini, A. Paralikis, N. Gregersen, and B. Munkhbat, "Single-Photon Emitters in WSe_2: Critical Role of Phonons on Excitation Schemes and Indistinguishability," *Physical Review B* 109, no. 24 (2024): 245304.

14. E. Blundo, C. Di Giorgio, G. Pettinari, et al., "Engineered Creation of Periodic Giant, Nonuniform Strains in $MoSe_2$ Monolayers," *Advanced Materials Interfaces* 7, no. 17 (2020): 2000621.

15. S. Ates, S. M. Ulrich, A. Ulhaq, et al., "Non-Resonant Dot–Cavity Coupling and Its Potential for Resonant Single-Quantum-Dot Spectroscopy," *Nature Photonics* 3, no. 12 (2009): 724.

16. C. Bennenhei, M. Struve, S. Stephan, et al., "Polarized Room-Temperature Polariton Lasing in Elliptical Microcavities Filled with Fluorescent Proteins," *Optical Materials Express* 13, no. 9 (2023): 2633.

17. B. Han, J. M. Fitzgerald, L. Lackner, et al., “Infrared Magnetopolaritons in $MoTe_2$ Monolayers and Bilayers,” *Physical Review Letters* 134, no. 7 (2025): 076902.

18. V. N. Mitryakhin, A. Steinhoff, J.-C. Drawer, et al., “Engineering the Impact of Phonon Dephasing on the Coherence of a WSe_2 Single-Photon Source via Cavity Quantum Electrodynamics,” *Physical Review Letters* 132, no. 20 (2024): 206903.

19. S.-J. Lee, H.-J. Chuang, A. L. Yeats, K. M. McCreary, D. J. O'Hara, and B. T. Jonker, “Ferroelectric Modulation of Quantum Emitters in Monolayer WS_2,” *ACS Nano* 18, no. 36 (2024): 25349.

20. L. Loh, Y. W. Ho, F. Xuan, et al., “Nb Impurity-Bound Excitons as Quantum Emitters in Monolayer WS_2,” *Nature Communications* 15, no. 1 (2024): 10035.

21. M. Abbarchi, M. Gurioli, A. Vinattieri, et al., “Phonon Sideband Recombination Kinetics in Single Quantum Dots,” *Journal of Applied Physics* 104, no. 2 (2008): 023504.

22. J. Suffczyński, A. Dousse, K. Gauthron, et al., “Origin of the Optical Emission within the Cavity Mode of Coupled Quantum Dot-Cavity Systems,” *Physical Review Letters* 103, no. 2 (2009): 027401.

23. S. Barzanjeh, A. Xuereb, S. Gröblacher, M. Paternostro, C. A. Regal, and E. M. Weig, “Optomechanics for Quantum Technologies,” *Nature Physics* 18, no. 1 (2022): 15.

24. J. Kettler, N. Vaish, L. M. De L'epinay, et al., “Inducing Micromechanical Motion by Optical Excitation of a Single Quantum Dot,” *Nature Nanotechnology* 16, no. 3 (2021): 283.

Supporting Information

Additional supporting information can be found online in the Supporting Information section.

Supporting File: adom71658-sup-0001-SuppMat.pdf.